Final Technical Report

DE-FG02-03ER54711

Investigations of Solar Prominence Dynamics Using Laboratory Simulations

PI: P. M. Bellan, California Institute of Technology

1 Context

Significant progress has been made in recent years towards understanding solar corona phenomena, yet many important problems remain, for example:

1. The coronal heating problem - why does the solar corona blatantly violate the second law of thermodynamics by having a temperature more than two orders of magnitude hotter than the photosphere?
2. The coronal loop uniformity problem - why is the cross-section of coronal loops approximately constant along the length of a loop? Coronal loops are arched magnetic flux tubes with footpoints anchored in the photosphere. Potential and force-free models, the most widely used models of magnetic structure, predict that the coronal loop axial magnetic field B_{axial} should become weaker with distance from the photosphere. This implies that the loop cross-section A should be larger at the apex than at the footpoints because flux conservation implies $A \sim B_{axial}^{-1}$. The fact that A is nearly the same at the apex as at the footpoints casts serious doubt on the validity of using either potential or force-free models (Fuentes *et al.* , 2006) to model coronal loops.
3. The triggering problem - why do coronal loops erupt suddenly? It is unclear whether eruptions are triggered by some slight internal change or by some external event.
4. The power supply problem - what is the energy source for the non-potential magnetic fields in the solar corona? Twisted magnetic fields have more internal energy than non-twisted (i.e., potential) fields satisfying the same boundary conditions. It is conventionally assumed in numerical magnetohydrodynamic (MHD) simulations that the twisting of coronal loops results from differential motion at the photospheric surface but recent detailed measurements (Pevtsov *et al.* , 2003) show that actual photospheric footpoint motion is much too small to account for the observed twist.
5. The particle acceleration problem - what accelerates particles to high energies in an eruption? Solar coronal physics is typically modeled using ideal MHD, an approximation where it is assumed that no electric field component exists parallel to the magnetic field. As a result, MHD models are incapable of predicting generation of energetic particles. In stark contrast to this 'non-prediction' by MHD, observations show that a considerable fraction of the stored magnetic energy in twist is transformed into the production of energetic particles and X-rays.
6. The scale height and particle source problem - why is the plasma density in coronal loops greater than the surroundings? This elevated density is known to be comprised of plasma of photospheric origin. If the coronal loop magnetic fields were potential or force-free, there would be no other force than gravity and isothermal loops would be expected to be in hydrostatic equilibrium in which case the plasma density in the loop should decay exponentially with altitude as $\exp(-z/H)$ where $H = \kappa T/mg \sim 3 \times 10^7$ m is the gravitational scale height. However, actual loops are uniformly filled with plasma to heights exceeding 10^8 m and so are uniform to altitudes exceeding $3H$ in extreme disagreement with the hydrostatic equilibrium prediction that the density should decay to $e^{-1} = 0.37$ of its surface value at a height $z = H$. The density at the apex of these high loops is thus more than 20 times greater than predicted by hydrostatic equilibrium models. This indicates the presence of strong upward forces that overwhelm gravity; neither force-free nor potential magnetic fields can provide such forces.

2 Existing approaches for studying solar corona physics

Four main methods, listed below in approximate historical order, have traditionally been used to study the solar corona and associated geo-effective events, namely:

Ground-based observation, the oldest method, continues to be effective. Solar telescopes (e.g., Big Bear, Sunspot, Tenerife) provide comprehensive, high-resolution coverage of the solar corona and have enabled discovery of many critical phenomena. The new Advanced Technology Solar Telescope (to be sited at Haleakalā, Hawaii) will use adaptive optics to provide much higher resolution than now available and so should provide yet more important discoveries in the future. Ground-based instrumentation also provides a means for measuring the solar magnetic field and vector magnetographs now enable measurement of the normal electric current density J_z. The ratio α of $\mu_0 J_z$ to normal magnetic field B_z is a critical parameter for theoretical models and recently regions where α reverses polarity have been correlated with flare location (Hahn *et al.* , 2005).

Analytic modeling became feasible after it was realized that the solar corona was a magnetized plasma. This meant that the solar corona could be modeled using known plasma theory, especially magnetohydrodynamics (MHD). During the last two decades MHD concepts such as Taylor relaxation (Taylor, 1974; Taylor, 1986), magnetic helicity, and magnetic reconnection have been successfully used to describe aspects of solar coronal plasma behavior.

Spacecraft such as SOHO, Yokhoh, TRACE, and Hinode have provided many new insights regarding the solar corona by accessing x-ray wavelengths that cannot penetrate the Earth's atmosphere and so cannot be studied by ground-based telescopes. Recent spacecraft images indicate much more fine-scale structure exists than envisaged a generation ago and also that this fine-scale structure can be highly dynamic.

Numerical simulations exploit ongoing large increases in computational power to produce visual representations of complex magnetic fields relevant to coronal observations. These simulations typically solve the ideal MHD equations over a 3D grid with tangential velocity and normal magnetic field specified as boundary conditions on a surface representing the photosphere. Simulations to date typically ignore density variations by either assuming zero or uniform density. By varying boundary conditions, a wide range of configurations can be simulated and insight beyond what is feasible using analytic methods can often be obtained.

Each of these four methods has made substantial contributions to the understanding of solar phenomena, but each also has shortcomings. For example, both ground and spacecraft observations passively observe real solar events. Because these observations do not measure all relevant parameters and because the events are both complex and never exactly the same, modeling is very difficult. On the other hand, because analytic models invoke many idealizing assumptions to make analysis tractable, direct relevance to specific actual observations is usually lacking even though worthwhile new insights might be obtained. Spacecraft are expensive and difficult or impossible to reconfigure or repair once launched. MHD numerical simulations are constrained by the many assumptions implicit in MHD. Specifically, MHD simulations omit particle effects, omit electrostatic effects, omit high frequency waves, have limited spatial and temporal resolution, and typically incorporate highly idealized boundary conditions that may be oversimplifications.

3 Lab experiments

The four methods listed above constitute an ensemble of methods for studying solar coronal physics – each has advantages and shortcomings, but together the four methods provide a powerful synergism. The author has developed a new method, laboratory simulation of solar coronal phenomena, that can be considered to be a new ensemble member bringing a complementary set of advantages and shortcom-

ings. The rationale for developing laboratory simulation was realization of the great similarity between solar corona magnetic structures and a laboratory plasma configuration called the spheromak. The author is neither the first nor the only person to make this realization – the similarity between spheromak concepts and solar coronal physics has been exploited in many theoretical models, numerical simulations, and most recently in the interpretation of ground and space-based observations. Spheromak technology is well developed and modifying this technology to be applicable to solar physics is straightforward, consisting of locating the vacuum chamber wall far from the plasma and changing the symmetry of boundary conditions. As with solar plasmas, plasma dynamics in the experiments is subject to the constraint that $\mathbf{E} + \mathbf{U} \times \mathbf{B} = 0$, i.e., the constraint that magnetic flux is frozen into the frame of the *moving* plasma.

As mentioned above, the laboratory method has its share of advantages and shortcomings and care is required to avoid over-selling it. Advantages include the ability to replicate the topology and dynamics of observed solar structures in a highly reproducible manner, the ability to diagnose all physical parameters in principle, the ability to control initial conditions, and the ability to observe interactions between MHD and non-MHD physics such as generation of energetic particles and x-rays. The use of a real plasma means that the laboratory simulation is inherently self-consistent and correct. Shortcomings are mainly due to the lab plasma not being an exact scale model of solar phenomena so physics observed in the lab experiment might not be relevant to solar phenomena. In addition, setting up a successful experiment involves significant challenges such as designing and building apparatus that provide clean reproducible results, developing suitable diagnostics, and relating measurements to theoretical models in a useful way.

The controlled nature of the experiments means that proposed models can be subjected to stringent tests. In particular, because basic parameters such as magnetic field strength and electric current can be adjusted, the credibility of a model can be quickly tested. This experimental approach to solar physics gives an intuitive 'hands-on' feel for the various physical phenomena. Laboratory experiments can also be used to provide an excellent test for numerical MHD simulations since numerical simulations should be able to simulate at least the MHD aspects of a lab experiment.

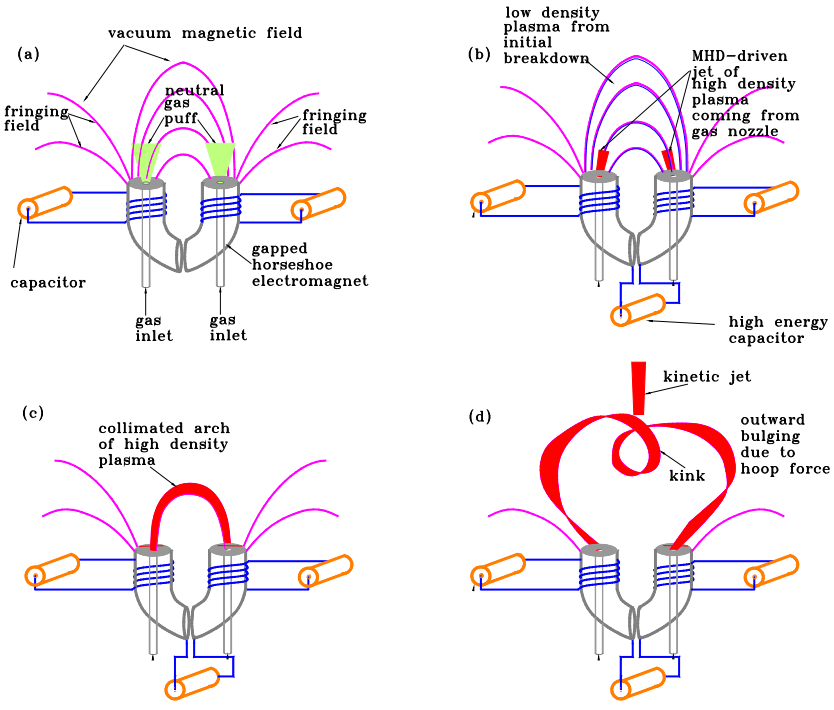

Figure 1: Sequence: (a) potential field established, neutral gas injected, (b) breakdown, upflows, (c) collimation, (d) expansion, kink, possible kinetic jet

4 Basic method

The basic experimental method is discussed here; extensions will be discussed later. Figure 1 sketches the typical sequence while Fig. 2 shows the actual configuration. In the first step of the sequence, a quasi-static 'horseshoe' electromagnet (Fig.1a) produces an initial arch-shaped potential magnetic field with field strength of the order of 1-3 kG at the footpoints. Next, sufficient neutral gas to enable breakdown is puffed via high-speed electromagnetic pulsed gas valves into the region between the magnet poles. After the gas puff, a high-energy capacitor bank charged to several kilovolts is connected across the magnet poles [see Fig.1(b)] and breaks down the neutral gas in about 0.1 μs to form a low density plasma as indicated in Fig. 1(b).

The initial current flowing through the tenuous plasma produced at breakdown is small and follows the arched vacuum field lines [Fig. 1(b)]. As the high-voltage capacitor discharges, this current increases to a peak value of 40-80 kiloamps in about 5-10 μs. The MHD $\mathbf{J} \times \mathbf{B}$ force associated with the current is observed to drive upflowing Alfvenic velocity plasma jets from both footpoints [see Fig. 1(b)]. These fast upflowing plasma jets quickly collide at the apex of the arched loop and fill the flux tube with plasma. The flux tube collimates as the two jets collide and then writhes to form a kink-like dip in the middle.

All the while, the magnetic hoop force causes an expansion of the major radius of the arch [see Fig. 1(d) and Fig. 2(right)]. The jet upflows and collimation were both unexpected effects that instigated development of a theoretical model (Bellan, 2003). This model motivated further experiments (You *et al.* , 2005) and these experiments provided verification for the flow/collimation model.

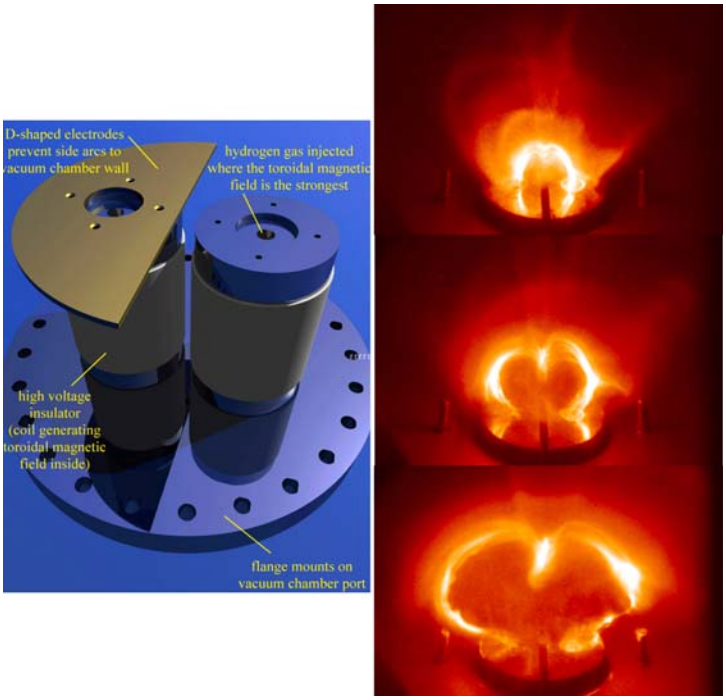

Figure 2: Left: configuration for creating single coronal loop (D-shaped electrode removed on RHS). Right: typical experimental lab simulations of single coronal loop

The sequence shown in Figs. 1 and 2(right) only occurs if neutral gas is provided at the nozzle; the gas is ionized at the nozzle and so provides a plasma source at the nozzle. Plasma density in the bright loop results from the flux loop being filled with plasma by the jet upflows; the loop plasma density is measured to be orders of magnitude larger than the density of the neutral gas initially puffed in to enable breakdown. The magnetic configuration thus depends on a mass flux boundary condition (i.e., plasma ingestion) as well as on the normal magnetic field and the normal electric current boundary conditions.

Nominal plasma parameters and ranges for hydrogen plasmas are listed in Table 1 (next page).

Parameter	Symbol	Value	Units	Parameter	Symbol	Value	Units
input power	P	60	MW	Alfvén velocity	v_A	3×10^5	m/s
input energy	W	1	kJ	Alfvén time	L/v_A	5×10^{-8}	s
plasma density	n	5×10^{20}	m^{-3}	resistive diffusion time	$\mu_0 L^2/\eta$	3.5×10^{-5}	s
temperature	T_e, T_i	2	eV	Lundquist number	$\mu_0 L v_A/\eta$	10^2	
gas		H		electron thermal vel.	v_{Te}	10^6	m/s
current	I	50	kA	ion thermal velocity	v_{Ti}	2×10^4	m/s
magnetic field	B	0.3	Tesla	electron Larmor radius	r_{Le}	1×10^{-5}	m
scale length	L	10	cm	ion Larmor radius	r_{Li}	5×10^{-4}	m
Coulomb log	$\ln\Lambda$	10		electron plasma freq.	f_{pe}	2×10^{11}	Hz
Debye length	λ_{De}	5×10^{-7}	m	ion plasma frequency	f_{pi}	5×10^9	Hz
resistivity	$\eta_{Spitzer}$	4×10^{-4}	Ohm-m	electron cyclotron freq.	f_{ce}	8×10^9	Hz
beta	β	4×10^{-3}		ion cyclotron frequency	f_{ci}	5×10^6	Hz

Table 1: Nominal parameters for hydrogen plasma coronal loop simulation experiment

5 Progress

5.1 Single coronal loop

A single loop system as described in Fig. 1 was constructed. This experiment (Bellan & Hansen, 1998; Hansen & Bellan, 2001) showed (i) frozen-in flux physics long thought to occur only on the sun could, in fact, be reproduced in the laboratory, (ii) the loop self-collimated almost instantly, (iii) the loop axis writhed in a helix, (iv) the surface projection was sigmoidal, (v) the major radius increased with time [see Fig. 2(right)], and (vi) plasma upflow from the electrodes affected magnetic field behavior.

5.2 Strapping field

A second, independent magnetic field system was arranged to provide a horizontal magnetic field $\mathbf{B}_{external}$ passing through the simulated coronal loop (see Fig. 3 top). The vertically directed $\mathbf{J}_{loop} \times \mathbf{B}_{external}$ force could, depending on the polarity of $\mathbf{B}_{external}$, aid or inhibit the tendency of the loop major radius to expand. Studies (Hansen & Bellan, 2001) of this multiflux system showed that loop eruption could be slowed or halted by application of a suitably strong $\mathbf{B}_{external}$ with appropriate polarity (see Fig. 3 bottom).

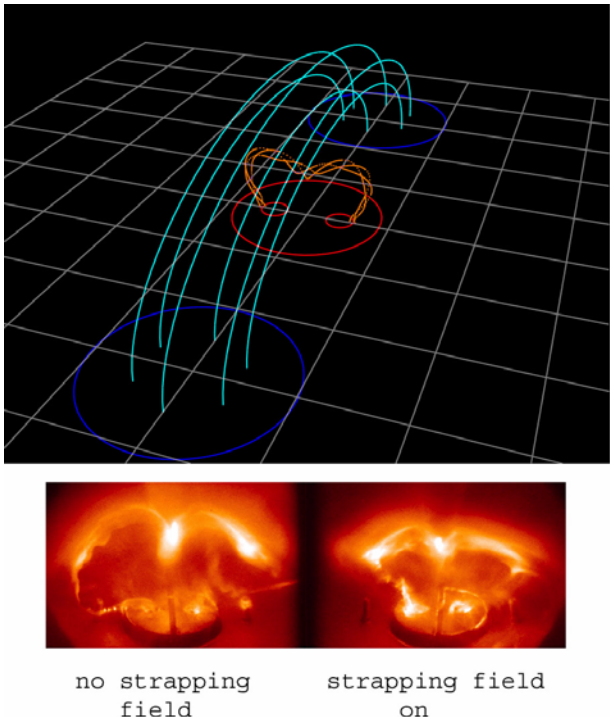

Figure 3: Strapping magnetic field (top, turquoise) inhibits upward expansion of loop (bottom right)

5.3 Co- and counter-helicity loop merging experiments

A system for creating two adjacent simulated coronal loops was constructed. These loops had parallel axial currents so they would always mutually attract. However, the axial magnetic field polarity was adjustable making it possible for the two loops to have the same or opposite chirality (i.e., co-helicity or counter-helicity).

Co- and counter-helicity merging experiments were dramatically different. Counter-helicity merging yielded a strong transient soft x-ray pulse (Hansen *et al.* , 2004) associated with annihilation of the oppositely directed axial magnetic fields. Eruption velocity increased after counter-helicity loops merged, presumably because annihilating axial magnetic field substantially reduces the field line 'tension' that normally restrains eruption.

5.4 Numerical MHD model

A numerical MHD model was developed using boundary conditions motivated by the experiment. This model was then extended (Tokman, 2001; Tokman & Bellan, 2002) to model coronal mass ejections and, as shown in Fig. 4, reproduced some detailed morphology of CME's.

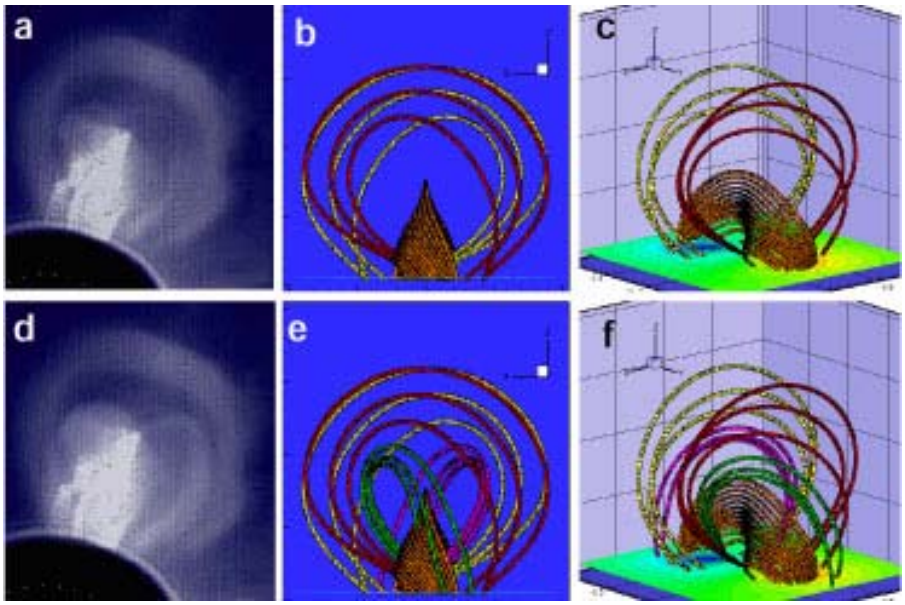

Figure 4: (a) beginning of CME, (b,c) beginning of numerical simulation, (d) later time showing heart pattern, (e,f) simulation showing heart pattern.

5.5 Spider legs

The early stages of a configuration used for astrophysical jet simulations involved an arcade of eight coronal loops arranged like the legs of a spider (see Fig. 5). These loops have the same helicity and merge to form a coaxial jet which then undergoes a dramatic kink instability (Hsu & Bellan, 2003; Hsu & Bellan, 2005). As seen in Fig. 5, these spider legs are very collimated (i.e., have axially uniform cross-section) in contrast to the dipole potential field existing before their formation.

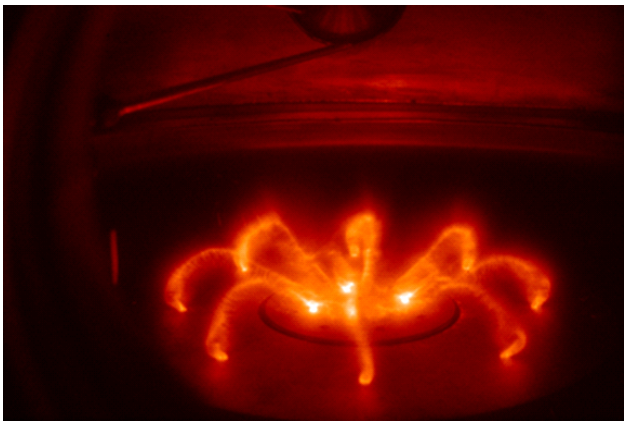

Figure 5: photo of "spider leg" array made using eight simulated coronal loops

5.6 Collimation model ('gobble' model)

A striking feature of all the experimental configurations was that current-carrying magnetic flux tubes quickly self-collimated, i.e., developed a uniform diameter along the axial length of the flux tube. Collimation was observed in the single coronal loop (see Fig. 2(right)), in the spider legs (see Fig. 5), and in the jet plasma resulting from the merging of the spider legs (Hsu & Bellan, 2005). A model developed to explain collimation (Bellan, 2003) shows that MHD forces associated with electric current flowing along an uncollimated magnetic flux tube always drive axial plasma flows from the thin to fat parts of the flux tube (the flux tube 'gobbles' plasma from the footpoints). As sketched in Fig. 6, these flows convect frozen-in azimuthal magnetic flux from the thin regions (ends) to the fat region (middle) where this flux accumulates thereby increasing azimuthal magnetic field B_ϕ which is the flux density. The increased B_ϕ pinches the fat midsection of the flux tube and so causes collimation. Collimation is thus associated with the flows filling the flux tube up with plasma. Examination of the induction equation (Bellan *et al.* , 2005) shows that $B_\phi/\rho r$ is invariant in the plasma frame so increasing ρ as a result of inflowing plasma necessarily increases B_ϕ and so causes pinching. In addition, stagnation of the flows heats the plasma. The model thus explains why bright flux tubes are hot, plasma-filled, and collimated. Uncollimated flux tubes do not kink because they lack the strong axial current required for kinking.

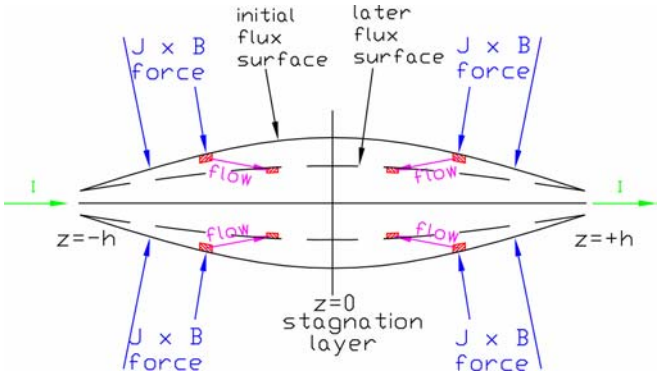

Figure 6: MHD-driven flows go from both footpoints to middle, pile up both plasma and embedded azimuthal flux, resulting in pinching and increased density.

5.7 Experiments verifying collimation model

The collimation model predicts that upflows from the footpoints of a flux tube should be associated with collimation. Fast ion gauge measurements of neutral density before breakdown and Stark broadening measurements of plasma density showed that the flux tube plasma density was essentially entirely due to upflow and definitely not due to ionization of pre-existing neutral gas. This result was published in Physical Review Letters (You *et al.* , 2005) and was the cover story as shown in Fig. 7. Recent multi-point spectroscopy by G. S. Yun (PhD thesis, July 2007) has provided more detailed flow velocity measurements as a function of axial position using Doppler shifts and Stark broadening measurements of the associated ρ increase; these detailed measurements are in good agreement with the collimation model.

Figure 7: PRL 7/22/2005

5.8 Kinetic jet

Early versions of the coronal loop simulation experiment occasionally manifested what looked like a conical spray of plasma shooting up from the apex of the loop as sketched in Fig.1d. This strange behavior which bears some similarity to jets of plasma shooting from actual solar loops was recently investigated in detail and was found to be a non-MHD effect. We called it a 'kinetic jet' to distinguish it from the 'MHD jet' driving the plasma upflow. The kinetic jet results from a particle orbit instability that occurs if the MHD jet accelerating plasma upflows from both footpoints is sufficiently strong. Ions in the MHD jet upflowing from the cathode footpoint move in the direction opposite the conventional current direction. It was found that if these counter-flowing ions move fast enough, then the qv_zB_θ magnetic force associated with this upflow can overwhelm the $qv_\theta B_z$ force that normally results in Larmor orbits and confinement to the flux tube. Thus, the fast counter-flowing ions are actually ejected from the flux tube via a magnetic force. Analytic and numerical models reveal this behavior in detail and predict a threshold for ejection of fast ions. Experimental measurements have confirmed this threshold (Tripathi *et al.* , 2007).

Figure 8(top) shows a sketch of a kinetic jet (conical structure shooting up from apex of loop), Fig. 8(middle) shows a photo of an argon loop with a kinetic jet (bright vertical structure), and Fig. 8(bottom) shows a hydrogen loop with no kinetic jet. Measurements of kinetic jet onset are in good agreement with a Hamiltonian model for particle motion in a helical magnetic field $\mathbf{B} = B_\phi\hat{\phi} + B_z\hat{z}$. The Hamiltonian model exploits symmetry to reduce the motion to 1D motion in a radial effective potential. This potential can be valley- or hill-like depending on parameters. The valley-like potential corresponds to conventional Larmor orbits with particles being confined to the flux tube in a manner consistent with conventional wisdom. However, the hill-like potential corresponds to a remarkable orbit instability whereby particles are expelled from the flux tube by magnetic forces so as to form the kinetic jet. Preliminary results have been published in Physical Review Letters (Tripathi *et al.* , 2007).

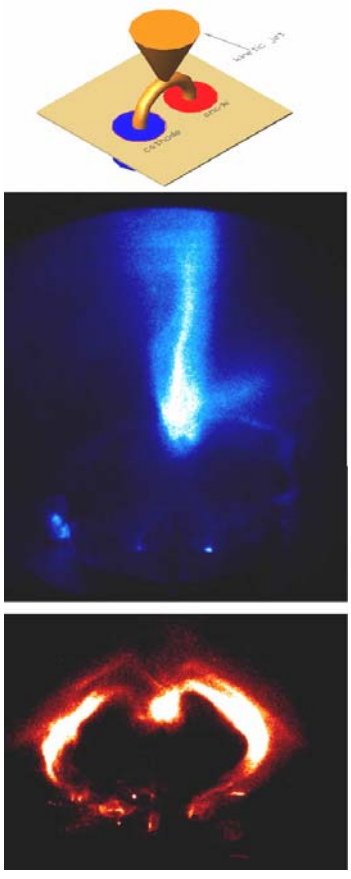

Figure 8: Top: sketch of kinetic jet. Middle: bright kinetic jet shooting out from top of dim argon loop. Bottom: Hydrogen loop with no kinetic jet

The kinetic jet involves a synergism between a helical magnetic field and fast particle motion in the negative v_z direction so that the outward v_zB_ϕ magnetic force becomes so strong as to overwhelm all other radial forces. An important counter-intuitive aspect of kinetic jets is that the stability of the trajectory of an ion traveling nearly on the z axis of a helical magnetic field depends on the sign of v_z. This has been verified by direct numerical solution of the equation of motion $md\mathbf{v}/dt = q\left[\mathbf{v}\times\left(B_\phi\hat{\phi} + B_z\hat{z}\right)\right]$ for the situation where B_z and J_z are uniform so $B_\phi \sim r$. Figure 9 plots this numerical solution for two particles starting at the same location near the z axis with $v_z = +v_0$ and $v_z = -v_0$ respectively and where v_0 exceeds a threshold value determined by a parameter S (Tripathi *et al.* , 2007) and $\lambda = \mu_0 J_z/B_z$. The particle with positive v_z stays near the z axis whereas the particle with negative v_z has an unstable trajectory and is expelled radially from the flux tube.

Kinetic jet ion velocities have been measured using spectroscopic blue shifts (Tripathi *et al.* , 2007) and are found to be quite energetic (several hundred eV). High speed movies suggest the kinetic jet ions are nearly unmagnetized because they fly off in a broad spray from the apex of the flux tube into a region where the magnetic field is at its weakest. The kinetic jet model (Tripathi *et al.* , 2007) assumed a straight cylindrical approximation to the flux tube geometry and so did not take into account that the magnetic field external to a collimated curved loop is weaker at the apex than at the footpoints. Since the kinetic jet instability involves fast ions escaping from a flux tube into a weak external magnetic field, it is expected that the kinetic jet should emanate from the loop apex where the external field is weakest.

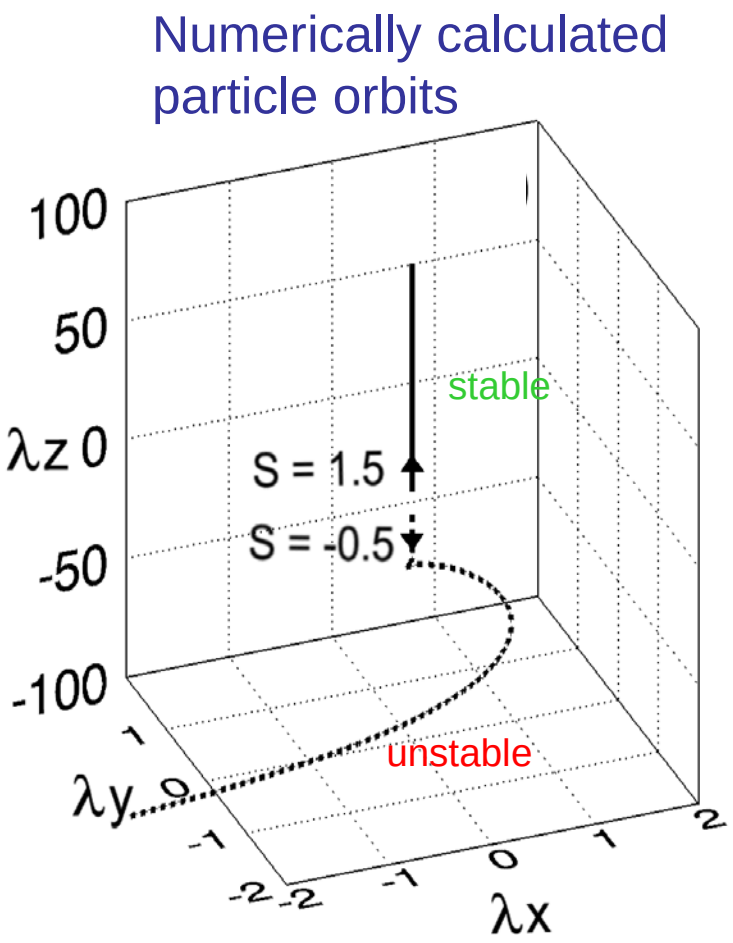

Figure 9: Trajectories of identical particles launched with same axial speed near z axis of helical magnetic field, but with opposite directions. Up-moving particle has stable trajectory, down-moving particle has unstable trajectory and is ejected from flux tube

References

BELLAN, P. M. 2003. Why helicity injection causes coronal flux tubes to develop an axially invariant cross-section. *Pages 1923–1929 of: Magnetic Helicity at the Sun, in Solar Wind and Magnetospheres: Vistas from X-Ray Observatories.* Advances in Space Research, vol. 32. 10.

BELLAN, P. M., & HANSEN, J. F. 1998. Laboratory simulations of solar prominence eruptions. *Physics of Plasmas*, **5**, 1991–2000. Part 2 Sp. Iss. SI.

BELLAN, P. M., YOU, S., & HSU, S. C. 2005. Simulating astrophysical jets in laboratory experiments. *Astrophysics and Space Science*, **298**, 203–209.

FUENTES, M. C. L., KLIMCHUK, J. A., & DEMOULIN, P. 2006. The magnetic structure of coronal loops observed by Trace. *Astrophysical Journal*, **639**(1), 459–474. Part 1.

HAHN, M., GAARD, S., JIBBEN, P., CANFIELD, R. C., & NANDY, D. 2005. Spatial relationship between twist in active region magnetic fields and solar flares. *Astrophysical Journal*, **629**(2), 1135–1140. Part 1.

HANSEN, J. F., & BELLAN, P. M. 2001. Experimental demonstration of how strapping fields can inhibit solar prominence eruptions. *Astrophysical Journal*, **563**, L183–L186. Part 2.

HANSEN, J. F., TRIPATHI, S. K. P., & BELLAN, P. M. 2004. Co- and counter-helicity interaction between two adjacent laboratory prominences. *Physics of Plasmas*, **11**, 3177–3185.

HSU, S. C., & BELLAN, P. M. 2003. Experimental identification of the kink instability as a poloidal flux amplification mechanism for coaxial gun spheromak formation. *Physical Review Letters*, **90**. Art. No. 215002.

HSU, S. C., & BELLAN, P. M. 2005. On the jets, kinks, and spheromaks formed by a planar magnetized coaxial gun. *Physics of Plasmas*, **12**. Art. No. 032103.

PEVTSOV, A. A., MALEEV, V. M., & LONGCOPE, D. W. 2003. Helicity evolution in emerging active regions. *Astrophysical Journal*, **593**(2), 1217–1225. Part 1.

TAYLOR, J. B. 1974. Relaxation of Toroidal Plasma and Generation of Reverse Magnetic-Fields. *Physical Review Letters*, **33**, 1139–1141.

TAYLOR, J. B. 1986. Relaxation and Magnetic Reconnection in Plasmas. *Reviews of Modern Physics*, **58**, 741–763.

TOKMAN, M. 2001. *Magnetohydrodynamic modeling of solar magnetic arcades using exponential propagation methods.* Caltech PhD thesis.

TOKMAN, M., & BELLAN, P. M. 2002. Three-dimensional model of the structure and evolution of coronal mass ejections. *Astrophysical Journal*, **567**, 1202–1210. Part 1.

TRIPATHI, S. K. P., BELLAN, P. M., & YUN, G. S. 2007. Observation of kinetic plasma jets in a coronal-loop simulation experiment. *Physical Review Letters*, **98**(13).

YOU, S., YUN, G. S., & BELLAN, P. M. 2005. Dynamic and stagnating plasma flow leading to magnetic-flux-tube collimation. *Physical Review Letters*, **95**. Art. No. 045002.

Appendix

Papers published as a result of this research grant

1. Large density amplification measured on jets ejected from a magnetized plasma gun , Yun GS, You S, Bellan PM

NUCLEAR FUSION Volume: 47 Issue: 3 Pages: 181-188 Published: MAR 2007

2. Observation of kinetic plasma jets in a coronal-loop simulation experiment, Tripathi SKP, Bellan PM, Yun GS,

PHYSICAL REVIEW LETTERS Volume: 98 Issue: 13 Article Number: 135002 Published: MAR 30 2007

3.Dynamic and stagnating plasma flow leading to magnetic-flux-tube collimation, You S, Yun GS, Bellan PM ,

PHYSICAL REVIEW LETTERS Volume: 95 Issue: 4 Article Number: 045002 Published: JUL 22 2005

4. Tendency of MHD forces to create localized, collimated plasma-filled flux tubes & ion orbit instability in a flux tube, Bellan PM, Yun GS, Tripathi SKP, et al.,

JOURNAL OF FUSION ENERGY Volume: 27 Issue: 1-2 Pages: 2-5 Published: JUN 2008

5.Co- and counter-helicity interaction between two adjacent laboratory prominences Hansen JF, Tripathi SKP, Bellan PM,

PHYSICS OF PLASMAS Volume: 11 Issue: 6 Pages: 3177-3185 Published: JUN 2004